The role of in situ generated morphological motifs and Cu(I) species in C_{2+} product selectivity during CO_2 pulsed electroreduction

Rosa M. Arán-Ais[1], Fabian Scholten[1], Sebastian Kunze[1], Rubén Rizo[1], Beatriz Roldan Cuenya[1 *]

[1] Department of Interface Science, Fritz-Haber-Institute of the Max-Planck Society, 14195 Berlin, Germany

***Corresponding Author:** roldan@fhi-berlin.mpg.de

Abstract

The efficient electrochemical conversion of CO_2 provides a route to fuels and feedstocks. Cu catalysts are well-known to be selective to multicarbon products although the role played by the surface architecture and the presence of oxides is not fully understood. Here, we report improved efficiency towards ethanol by tuning the morphology and oxidation state of the Cu catalysts via pulsed CO_2 electrolysis. We establish a correlation between the enhanced production of C_{2+} products (76 % ethylene, ethanol and n-propanol at -1.0 V vs RHE) and the presence of (100) terraces, Cu_2O, and defects on Cu(100). We monitored the evolution of the catalyst morphology by analysis of cyclic voltammetry curves and ex situ atomic force microscopy data, while the chemical state of the surface was examined via quasi in situ X-ray photoelectron spectroscopy. We show that the continuous (re-)generation of defects and Cu(I) species synergistically favors the C-C coupling pathways.

This document is a post-peer-review, per-copyedit version of an article published in Nature Energy. The final authenticated version is available online at https://doi.org/10.1038/s41560-020-0594-9.

Renewably-sourced electricity can be used to break and rearrange the bonds of CO_2 and water molecules into complex hydrocarbons, which in turn can be burnt to produce energy and CO_2 that can be again transformed, closing thereby the carbon cycle[1,2]. Among the catalytic materials studied so far to facilitate the CO_2 reduction reaction (CO_2RR), Cu is the only one that generates ethylene, ethanol and n-propanol (C_{2+} products) with significant yield[3–5].These products are highly valuable as feedstocks in the chemical industry and as fuels for transportation purposes[6]. Therefore, significant attention is currently devoted to unraveling the factors that determine the activity and selectivity of Cu-based catalysts[3,7–9].

The complexity of the CO_2RR arises from the multiple electron transfer steps involved and the strong surface structure sensitivity of the process. Previous theoretical[10–13] and experimental studies[14–16] have demonstrated that the C—C coupling pathway towards ethylene is favored on the Cu(100) surface. Recently, the catalytic role played by $Cu^{\delta+}$ and sub-surface oxygen has been noticed[17–24], as well as the positive effect of oxygenated surface species for alcohol production[25]. In this regard, the concurrence of Cu(I) and Cu^0 species at the electrocatalyst surface was predicted to lead to an enhancement of the CO dimerization[19]. Nonetheless, the stabilization of Cu(I) under operando CO_2RR conditions is very difficult, although it was recently shown on certain nanostructured materials[20,24], or when modifier elements that slow down its reduction were introduced[17,26]. However, minor control over the exposed facets of the traditional oxide-derived (OD) Cu catalysts can be achieved during their preparation, resulting in poly-oriented surfaces.

A well-defined surface structure and known composition are essential for the fundamental understanding of the parameters controlling CO_2RR selectivity. For instance, an anodic pulse applied to a single crystal electrode at a selected potential allows the generation of adsorbed oxygen or oxidized surface species that can be involved in the CO_2RR occurring during the subsequent cathodic pulse. Although some works exist on pulsed-mode electrolysis during CO_2RR over Cu[25,27–33], their product selectivity data revealed a main enhancement towards CO and CH_4 production, with ethanol not being analyzed in most cases. Furthermore, no direct experimental evidence of the factors leading to the different reactivity was provided.

Here, we describe the simultaneous effect of having well-defined surface structures and Cu(I) species in the reaction pathways that yield C_{2+} products. By rationally designing the pulsed potential sequence applied, we were able to simultaneously tune the surface structure and composition of the Cu catalysts during CO_2RR. In particular, Cu(100) surfaces with known defect structures and different ratios of Cu^0 and Cu(I) species have been studied and their role in the product selectivity illustrated.

Structure sensitivity of the oxide formation. Characteristic fingerprints of distinct surface arrangements can be obtained from cyclic voltammograms (CVs) acquired on different Cu single crystal electrodes in different electrolytes. Given the favored C—C coupling on the special square configuration of Cu(100), we have focused our study on this surface orientation. The detailed description of the voltammetric profiles of Cu(100) and a Cu foil (polyoriented surface) is provided in Supplementary Note 1 and Supplementary Figures 1 and 2a. Such study is needed in order to select the potentials at which a desired oxidation state of the Cu surface is achieved. It is assumed that the formation of Cu_2O takes place above 0.3V vs RHE with a well-defined peak around 0.6V for all surfaces, while above 0.8V the formation of CuO is presumed[30,34]. Considering the aforementioned potentials, a pulse sequence was used for CO_2RR on the Cu(100) electrode in order to achieve control over both, surface structure and composition. Supplementary Figure 2b shows the alternated voltage program applied: a brief pulse at an anodic potential (E_a) was followed by a pulse at a cathodic potential typically used for CO_2RR (E_c=-1.0V), repeating this sequence for 1h. In order to selectively generate different surface species, the E_a was varied from 0 to 0.8V (arrows in Supplementary Figure 2a). Anodic pulses (t_a) of 1s followed by cathodic pulses with different lengths (t_c) were applied in this study. Such pulses were sufficiently long to induce changes in the surface composition (transient curve shape, Supplementary Figure 3).

Morphological changes monitored by atomic force microscopy. The surface structure of Cu electrodes strongly depends on the pre-treatment[35] and reconstructions take place under CO_2RR[36–38]. Figure 1 and Supplementary Figure 4 show clear differences in the morphology of the differently-treated samples (Supplementary Note 2). When the reaction is carried out under potentiostatic conditions, the initial flat surface becomes ‘granular’ (Figure 1a), but with a much smaller overall roughness than that

of the 1h pulsed surfaces, whose roughness differs drastically depending on the specific pulse protocols applied. The large structures observed in Figure 1c,e are produced by the continuous oxidation/reduction (dissolution/redeposition) of copper. These cubic islands can be considered as (100) facets terminated by step-edge defects. Applying 1h of pulsed electrolysis followed by 1h of constant potential (-1.0V vs RHE), Figure 1f, leads to a surface where the cubic structures are still visible, but are less well-defined, illustrating that some of the defects created during the pulse treatment have been healed. From these images it is evident that although some morphological changes already take place at $E_a \leq 0.4$V (Figure 1b and Supplementary Figure 4d), the main structural modifications occur when higher positive potentials are applied (Figure 1c-f).

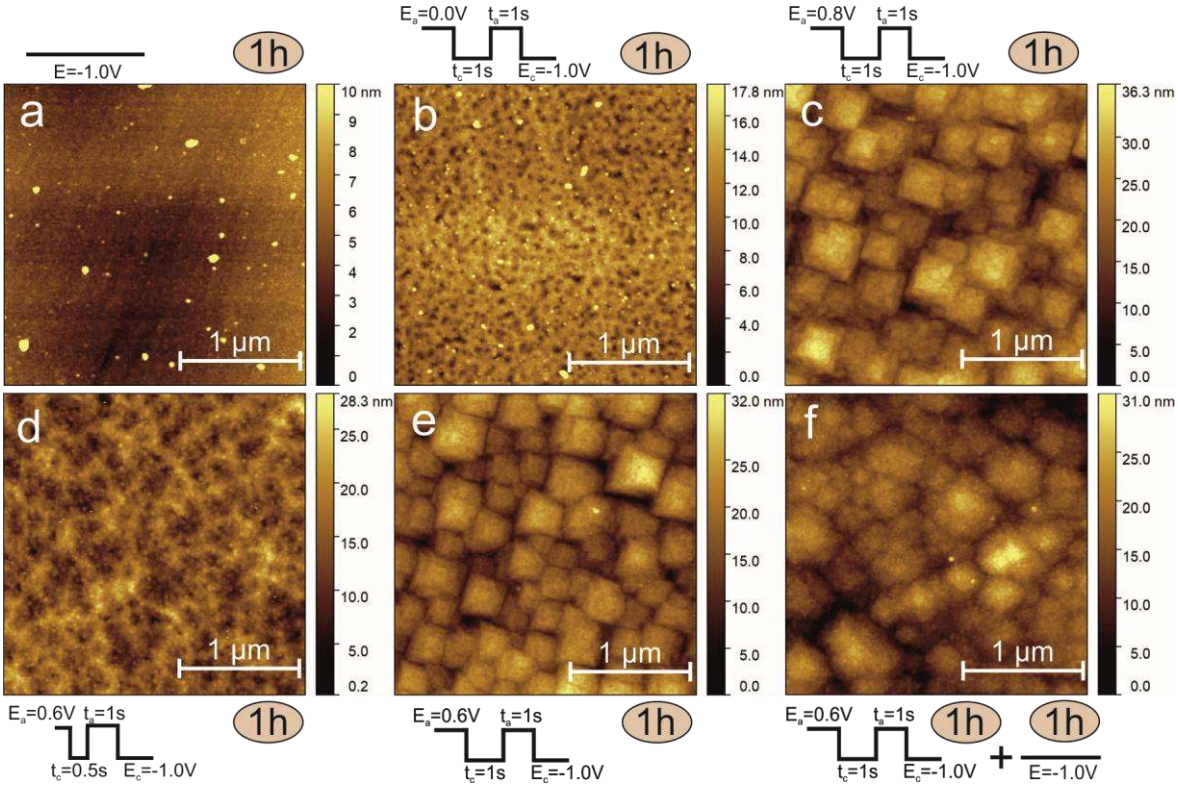

Figure 1. Atomic force microscopy (AFM) images of a Cu(100) electrode after different surface treatments and reaction settings. Each panel shows the electrode after 1 h electrolysis under the following conditions: **a,**constant potential of -1.0 V vs. RHE; pulsed electrolysis **b,** E_a = 0.0 V, E_c = -1.0 V, $t_a = t_c$ = 1 s; **c,** E_a = 0.8 V, E_c = -1.0 V, $t_a = t_c$ = 1 s; **d,** E_a = 0.6 V, E_c = -1.0 V, t_a = 1 s, t_c = 0.5 s; and **e,** E_a = 0.6 V, E_c = -1.0 V, $t_a = t_c$ = 1s. **f,** shows the surface from panel **e** after a subsequent hour of potentiostatic electrolysis at -1.0 V vs. RHE.

Quasi in situ X-ray photoelectron spectroscopy. To confirm the identity of the surface species resulting from the application of different step potentials, Cu LMM Auger electron spectra (AES) were acquired on the electropolished (EP) Cu(100) electrode after holding the potential for 5min at E_a, Supplementary Figure 5a. Spectra deconvolution provided surface chemical composition and distinction between metallic Cu and Cu(I) species. Additionally, O1s and C1s X-ray photoelectron spectroscopy (XPS) spectra were also analyzed, Supplementary Figure 5b,c. The Cu surface is fully metallic when exposed to the constant reducing -1.0V working potential. Within the anodic potentials studied, the spectrum acquired at E_a=0.0V displays 2% Cu_2O, which is within our error margin of Cu(I) determination and rather reflects the hydroxylation of the surface. Cu_2O was already formed at 0.4V, although in a smaller amount (15%) as compared to that present at higher potentials (0.6V and 0.8V), with roughly 46% Cu_2O. CuO species (9%) were only observed after the pulse at 0.8V (Supplementary Table 1).

To gain further insight into the stability of the different $Cu^{\delta+}$ species under reaction conditions, the same pulsed protocol used in CO_2RR selectivity measurements was applied (t_a=t_c=1s, E_c=-1.0V, E_a=0.0, 0.4, 0.6 and 0.8V). The Cu LMM AES spectra were then collected after stopping the alternated potential sequence either at the upper (E_a, Figure 2a) or lower (E_c, Figure 2b) potential pulses. The amount of Cu_2O formed at E_a within 1s pulse is lower than after 5min of applied potential but still considerable, and the Cu_2O coverage is proportional to E_a. Only 4% of CuO was detected for E_a=0.8V after the 1s pulse. Interestingly, when the reaction is stopped at the reducing potential pulse (E_c=-1.0V, t_c=1s, Figure 2b), the oxides created in the previous anodic pulse are not fully reduced, indicating that Cu_2O species (7-11%) are still present during the cathodic pulse when CO_2RR takes place. Similar conclusions can be drawn when looking at the O1s spectra (Figure Supplementary 6).

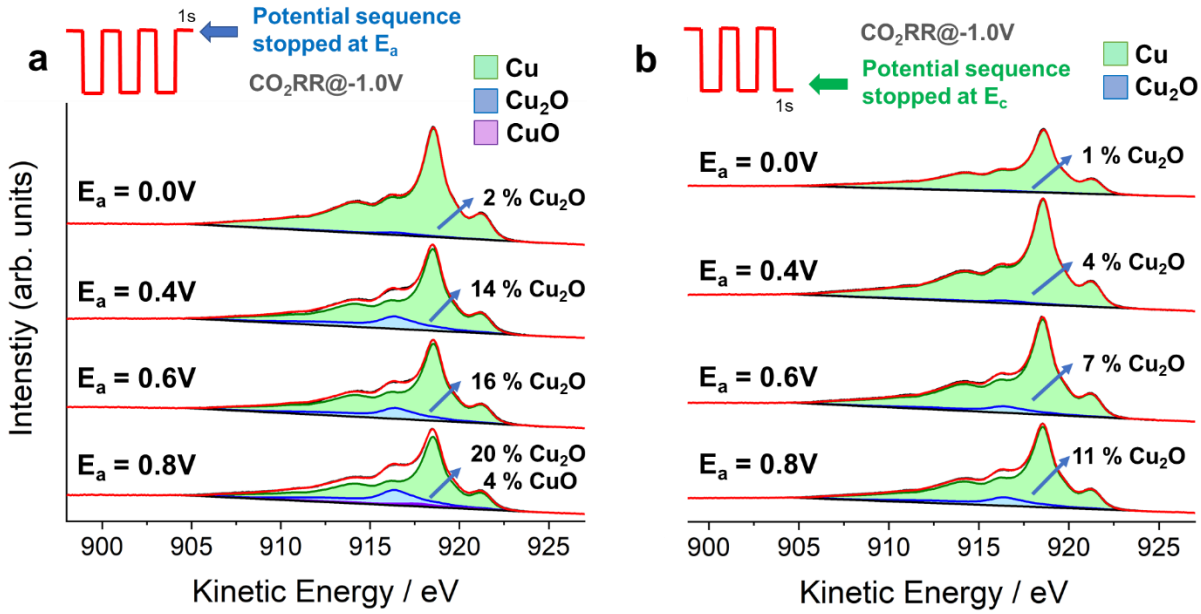

Figure 2. Quasi in situ Cu LMM Auger spectra of a Cu(100) electrode after the different pulse protocols indicated. All spectra were acquired after 1 h of pulsed electrolysis in CO_2-saturated 0.1 M $KHCO_3$ solution after stopping the 1s square wave potential sequence after the **a,** upper/anodic (E_a vs RHE) and **b,** the lower/cathodic pulses (E_c = -1.0 V vs RHE). Cu_2O and CuO amounts were estimated from the integrated area of the fit with the corresponding reference spectra.

Catalytic reactivity under pulsed conditions. We next sought to establish correlations between surface structure, composition, and CO_2RR selectivity. In addition to the AFM analysis, cyclic voltammetry was used to qualitatively distinguish structural modifications of the Cu(100) electrode after the pulsed experiments (Figure 3). One difficulty in pulsed electrolysis arises from the complicated differentiation between the non-faradaic transient current and the faradaic reaction current processes, which makes the faradaic efficiency (FE) determination inaccurate and unreliable. For this reason, we report the CO_2RR product selectivity as a percentage of the total charge employed during the electrolysis to generate all detected products[29].

Figure 3 shows strong differences in the CO_2RR outcomes derived from the different surface compositions achieved by pulsed electrolysis, together with the different surface reconstructions determined from the changes observed in the CVs and the AFM images. Even though the overall voltammetric profile of the Cu(100) electrode does not show prominent changes after CO_2RR[16,25] when

applying a constant negative potential of -1.0V, certain surface reconstruction cannot be completely excluded (Supplementary Figure 7). As indicated by quasi in situ XPS, the Cu(100) surface remains mostly metallic when the voltage is alternated between -1.0V and the first upper potential studied (0.0V). Minor surface rearrangement was found at this E_a (Figure 1b and 3), and a similar product distribution to that obtained under potentiostatic conditions. The modest increase in ethanol observed for E_a=0.0V is in agreement with a previous study that associated it to a higher OH coverage at the Cu surface[25].

In contrast, we have shown that Cu_2O is already present on the Cu surfaces when pulsing at E_a=0.4V (~14%) for 1s, and that this oxide is not completely reduced during the consecutive CO_2RR reductive step at -1.0V for 1s (~4%). Therefore, the Cu(I) species are available on the surface during the reducing pulse and continuously (re)generated during the following E_a pulse. Interestingly, a clear increase in ethanol selectivity is observed when metallic Cu and Cu(I) species coexist at the surface during CO_2RR. For instance, 24 % ethanol production is reached by biasing at E_a=0.4V, accompanied by a decrease in ethylene selectivity (27%), while 32% ethanol and a total of 76% of C_{2+} products were obtained for E_a=0.6V. For reference, the same EP Cu(100) electrode measured under constant potentiostatic conditions at -1.0V lead to 8% ethanol and 45% ethylene. These results point out a deviation from the pathway that leads to ethylene formation towards the route yielding ethanol as a result of the in situ modification of the surface structure as well as the chemical composition of the Cu surface induced by the pulses. Moreover, Figure 3 shows that the hydrogen evolution reaction (HER) is significantly suppressed when pulsing at 0.6V for 1s (<10% selectivity, also for E_a=0.8V). It is known that the positive polarization of the electrode lowers the surface hydrogen coverage, thus leading to a lower hydrogen selectivity[39]. Higher OH coverage is also expected at this E_a, thus favoring the pathway towards ethanol formation.

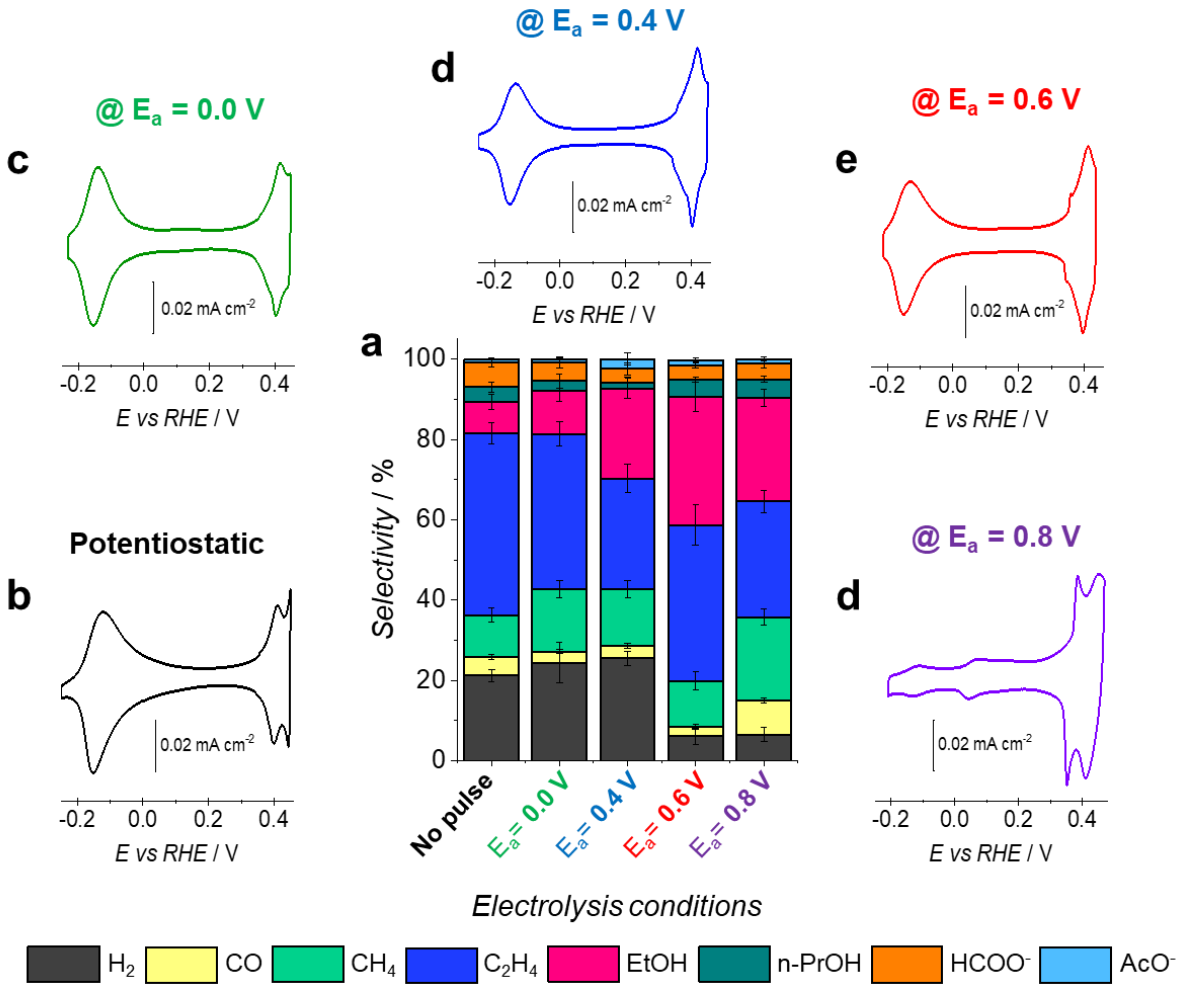

Figure 3. CO_2 pulsed electrolysis on a Cu(100) single crystal. a, Bar chart shows the product selectivity (%) at a constant voltage of -1.0 V vs RHE (no pulse) and pulsed conditions with different applied E_a. The selectivity was acquired after 1 h of CO_2RR in 0.1 M $KHCO_3$ at E_c = -1.0 V, with $t_a = t_c$ = 1 s, and corresponds to an average of at least three different measurements. The error between experiments is given as the standard deviation. **b-d,** Voltammetric profiles of the Cu(100) electrode after reaction under potentiostatic and pulsed electrolysis under different E_a conditions. Cyclic voltammetry was performed in an Ar-saturated 0.1 M NaOH solution at a scan rate of 50 mV s^{-1}.

Our experimental data demonstrate that the pulses lead to morphological as well as chemical changes in the Cu(100) surface. A previous study on stepped Cu single crystal surfaces showed that the increased charge density detected in the CVs of Cu(100) above 0.3V can be associated to the presence of (111) steps or defects on this surface orientation[40]. The CVs recorded for E_a of 0.4 and 0.6V (Figure 3) differ from the one recorded for the EP Cu(100), displaying higher charge above 0.3V, and therefore, a higher

defect density. In fact, they resemble an overlap between Cu(911)[40] and Cu(310) stepped surfaces, Supplementary Figure 8. Nonetheless, although the CVs are rather similar, the product distribution in all cases is different, namely higher C_{2+} selectivity for pulsed Cu(100) with E_a=0.6V. The AFM images acquired after reaction (Figure 1 and Supplementary Figure 4) for the pulsed samples clearly point out different surface morphology and roughness. The observed surface reconstruction is supported by previous studies based on operando electrochemical scanning tunneling microscopy (EC-STM)[36–38].

More pronounced surface restructuring is observed for the Cu(100) electrode when pulsing at 0.8V, as deduced from the strong changes in the CV, which after this pulsed sequence displays the characteristic voltammogram previously obtained for a polycrystalline Cu foil (Supplementary Figure 1a). Similar selectivities for CO, CH_4 and C_2H_4 than those of a Cu foil at -1.0V are obtained, but with HER suppression in favor of higher ethanol selectivity for the pulsed Cu(100) (E_a=0.8V). Quasi in situ XPS revealed that Cu_2O predominates at this E_a, with only a minor concentration of CuO (4%) being found after 1s of oxidative pulse. Under these circumstances, the CO_2RR takes place on highly defective surfaces containing also Cu(I) species. The well-ordered domains of the EP Cu(100) electrode are progressively destroyed by the E_a=0.8V pulses and ethylene production decreases when the (100) terraces are gradually populated by a high defect density. Moreover, a decrease in ethanol selectivity was also observed, contrary to the higher production that is usually observed on highly defective and oxidized Cu materials. Limited C—C bond formation on short (100) terraces was previously reported for both CO and CO_2 electroreduction[15,41]. Therefore, our results indicate that the enhanced C_{2+} product yield arises from the synergistic combination of having wide (100) domains populated by defects, and sufficiently stable Cu_2O surface species.

Surface defects *vs* Cu(I). Enhanced C_{2+} product yield of Cu electrodes has been previously linked to the presence of optimal morphological features (defects[15], grain boundaries[42] and roughness[43]), and to concomitant changes of the local pH[13,44]. Although the changes in the electrochemically active surface area (ECSA) resulting from the applied anodic pulses have been estimated almost negligible (Supplementary Table 2), it is known that the presence of steps diminishes the activation barrier for CO_2

dissociation on Cu(100)[47], which must be at least partially related to the observed experimental improvement towards C_{2+} product selectivity[15,48].

To address the open question of whether the enhanced CO_2R selectivity comes exclusively from the induced surface defects versus the concomitant presence of the in situ (re-)generated Cu_2O , we run the pulsed electrolysis on the Cu(100) electrode and subsequently on the resulting defective surface but at constant potential (-1.0V). The pulsed program at E_a=0.6V changes the well-ordered (100) domains, and the altered surface (red curve in Figure 4a) also experiences some slight additional changes at a constant potential of -1.0V (green curve Figure 4a). Such changes are better identifiable by AFM (Figure 1), but in both cases the surface roughness and defect content remains similar.

Conversely, Figure 4b shows that the in situ (re)-generation of Cu(I) has a clear impact in the selectivity towards C_{2+} products, since it decreases by 37% (t_c=1s) when the "defective Cu(100)" electrode is not pulsed but measured under potentiostatic conditions. Interestingly, similar results were obtained for shorter cathodic pulses (t_c=0.5s, Figure 4b and Supplementary Figure 9). Therefore, even when defects are present on the Cu(100) surface, C_1 products and HER are still more favored when the reaction is carried out at constant potential and Cu(I) species are absent. In fact, the large changes in selectivity obtained under pulsed conditions might be attributed to the distinct chemical environment of the electrode under pulsed (coexistence of Cu(I) and Cu^0 and higher surface oxophilicity) *vs* potentiostatic conditions that constrains the HER in favor of ethanol production in the former experiments.

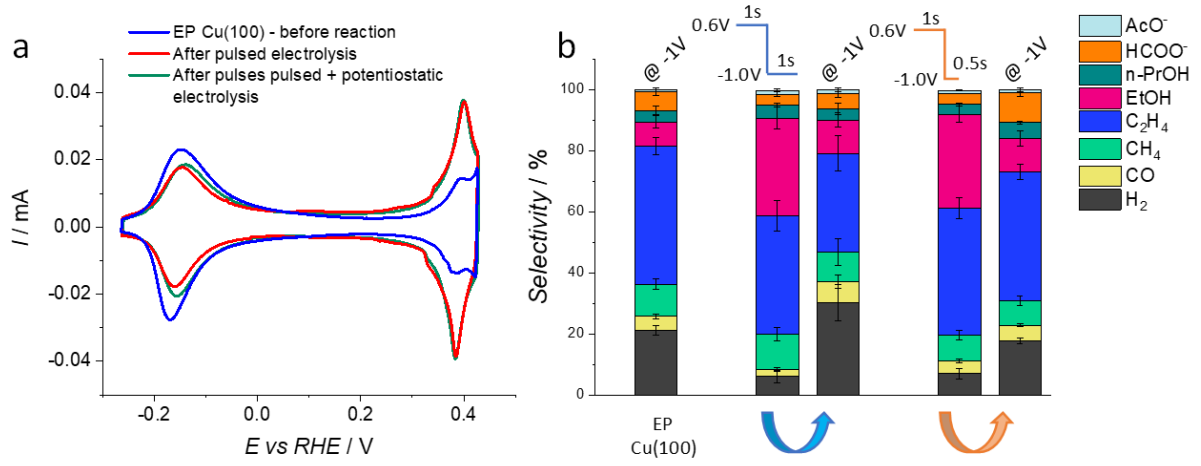

Figure 4. Surface defects *vs* Cu(I) for C_{2+} production. a, Voltammetric profiles of the EP Cu(100) electrode, the Cu(100) with defect sites created in the pulsed electrolysis (E_a = 0.6 V, E_c = -1.0 V, $t_a = t_c$ = 1 s), and the same defective Cu(100) surface after a subsequent CO_2 electroreduction under constant potential conditions (-1.0 V). CVs were recorded in 0.1 M NaOH at 50 mV s^{-1}. **b,** Product selectivity of the aforementioned surfaces under potentiostatic (- 1.0 V) or pulsed conditions. Product selectivity for t_c = 0.5 s are also included for comparison. Arrows indicate that the resulting surface from the pulsed electrolysis was subsequently measured at a constant potential of - 1.0 V. The selectivity data reported are an average of at least three different measurements and the error is given as the standard deviation.

Figure 5a displays structure-selectivity correlations, where the $Q_{defects}/Q_{100}$ ratio, used to evaluate the defect density on the Cu(100) electrode (Supplementary Note 3), as well as the % of ethanol and ethylene produced have been plotted for the different surfaces analyzed. The FE for Cu(911) and Cu(310) taken from literature[15] are also plotted for reference. The effect of the defect density and surface oxide content was also studied by testing the cathodic pulse duration, t_c. In the case of the Cu(100) electrode, the results under pulsed conditions (E_a=0.6V, E_c=-1.0V, t_a=1s, t_c=1, 0.5 and 0.2s) are displayed together with the ethanol FE of the resulting defective surface measured subsequently under potentiostatic conditions (-1.0V).

As expected, the EP Cu(100) has the lowest defect density. A slightly higher reconstruction is produced when shorter pulses are applied. Interestingly, similar $Q_{defects}/Q_{100}$ ratio are obtained for the pulsed pre-treated Cu(100) (E_a=0.6V, E_c=-1.0V, t_a=1s and t_c=0.5 and 0.2s) and the Cu(911) electrode, which all display similar ethanol FE when the reaction is run under potentiostatic conditions (-1.0V). However, higher ethanol selectivity is obtained when the Cu(100) surface is continuously (re-)oxidized (pulsed CO_2RR). Moreover, comparable high FE for ethanol was observed for the Cu(310) electrode under potentiostatic conditions, which is assigned to the higher Q_{defect}/Q_{100} ratio in comparison to the pulsed Cu(100) electrode. These results highlight that the morphology changes caused by the pulses cannot be solely responsible for the higher ethanol selectivity, but that the continuously re-generated

Cu(I) species must also be considered, since the pulsed surfaces with much lower defect density than Cu(310) result in similar ethanol FE when Cu(I) species are present.

A different trend, although not as clear, is observed for ethylene: surfaces with the smallest content of (100) motifs, Cu(310) and Cu poly, show the lowest ethylene production, and no improvement is observed in the ethylene yield of Cu(100) when comparing pulsed versus potentiostatic reaction conditions. Our data in fact suggest that the ethylene pathway is dominated by the presence of (100) motifs and not as much by the stabilization and re-generation of Cu(I) species, as was clearly the case for ethanol production.

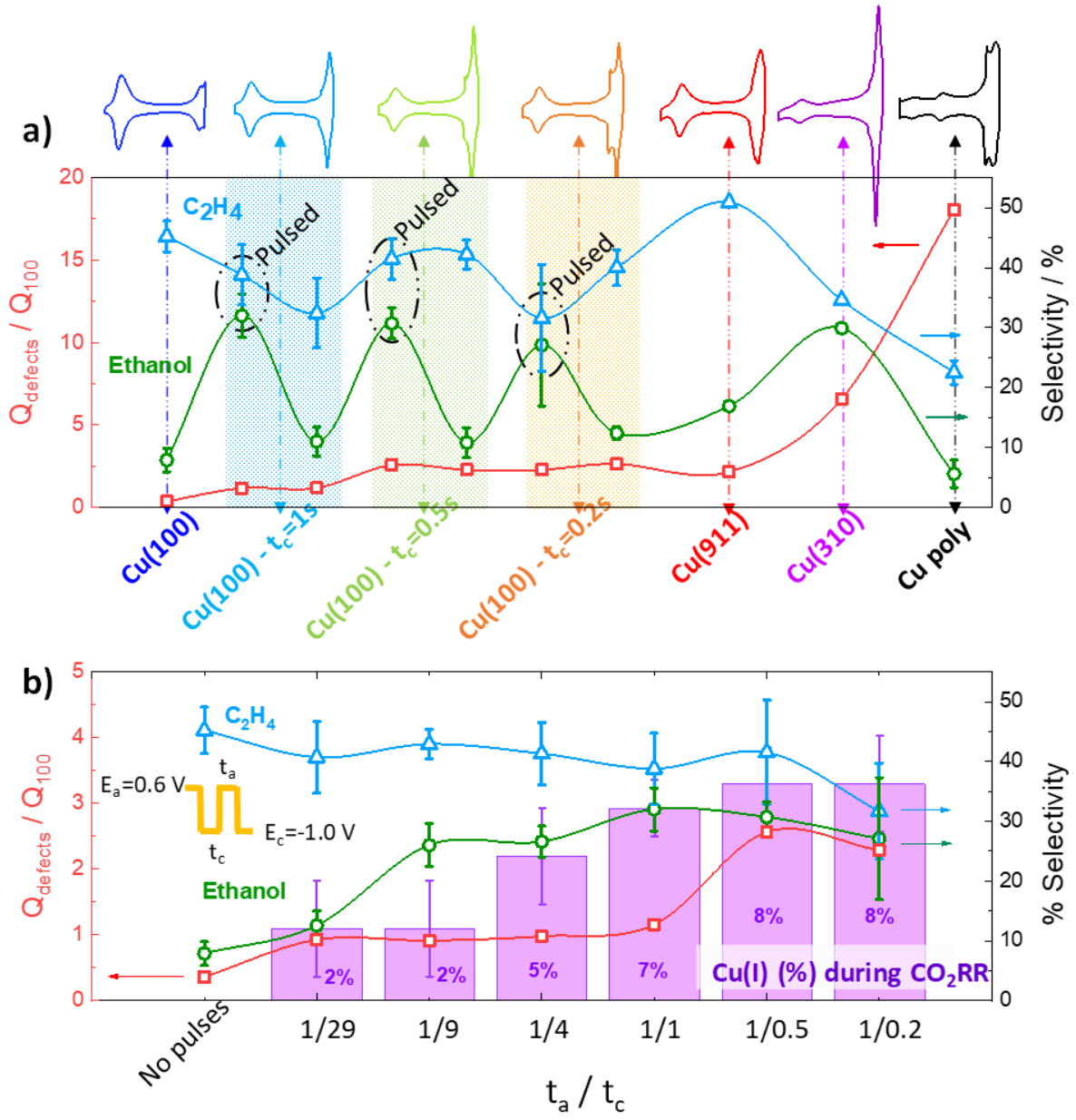

Figure 5. Defect density vs product selectivity. $Q_{defects}/Q_{100}$ and product selectivity (%) as a function of **a**, Pulsed vs potentiostatic conditions for a Cu(100) electrode, including Cu stepped surfaces for comparison. Top row shows the voltammetric profiles recorded in 0.1 M NaOH (50 mV/s) of the Cu surfaces evaluated after 1 h CO_2RR in CO_2-saturated 0.1 M $KHCO_3$ and denoted in the bottom row. Unless specified, measurements were performed at a constant potential of - 1.0 V. Measurements carried out under pulsing conditions (E_a = 0.6 V, E_c = - 1.0 V, t_a = 1 s and t_c as indicated, 1 h reaction) are labelled as "pulsed". The shaded areas encompass the measurements done under pulsed condition and

the consecutively potentiostatic one. **b,** t_a/t_c applied. Measurements carried out under pulsing conditions (E_a = 0.6 V, E_c = - 1.0 V, t_a/t_c as indicated, 1 h reaction). Bars indicate the surface Cu_2O content (%) determined by quasi in situ XPS when stopping the alternated potential sequence after the cathodic pulse for every t_a/t_c tested. Selectivity data is reported as an average of at least three different measurements and the error is given as the standard deviation.

In order to compare surfaces with similar defect density (identical pulse parameters E_a=0.6V, E_c=-1.0V and t_a=1s) but different content of Cu(I) species, the length of the t_c pulse was systematically varied, Figure 5b. The corresponding product distributions are shown in Supplementary Figure 10. The total percentage for ethylene and alcohols amounts 70-76% for all t_a/t_c tested. The ethanol yield was found to be higher for shorter t_c, when higher Cu_2O coverages were obtained, Supplementary Figure 11. Supplementary Figure 12 shows additional C-1s and O-1s spectra from the same samples. For longer t_c pulses (e.g. t_c=29s), when no Cu(I) was detected (values within the experimental error), the ethanol production was found to drastically decrease, accompanied by an increase of the hydrogen yield. Interestingly, ethylene production was favored when longer t_c were applied, i.e., when the surface was more metallic and larger Cu(100) domains were available.

Figure 5b shows the ratio $Q_{defects}/Q_{100}$ vs ethanol and ethylene selectivity for the different t_c tested (CVs of the resulting surfaces shown in Supplementary Figure 13). For t_c between 29 and 1s, similar $Q_{defects}/Q_{100}$ ratio is achieved, although displaying increasing ethanol selectivity as t_c becomes shorter, i.e. when higher Cu_2O coverage is available on the surface. The quasi in situ XPS analysis reveals a surface oxide saturation for $t_c \leq 1$s(Supplementary Figure 11), which has associated a similar ethanol selectivity , regardless of the morphology (higher $Q_{defects}/Q_{100}$ ratio for shorter t_c). Regarding ethylene selectivity, Figure 5b points out a clear relationship between the content of (100) motifs and the ethylene production.

Differential electrochemical mass spectroscopy measurements. Figure 6 shows the linear sweep voltammetries (LSV) and the mass to charge signals (m/z) for the fragments associated to methane

(CH_3^+, m/z=15), ethylene ($C_2H_2^+$, m/z=26), alcohols (CH_3OH^+, m/z=31) and hydrogen (m/z=2) formation during the CO_2RR. Methanol, ethanol and n-propanol species can be responsible for the m/z=31 fragment. However, it is worth mentioning that no methanol was detected by our chromatographic methods during the different experiments (also in agreement with the literature) and therefore, only ethanol and n-propanol are expected to contribute to this signal.

First, the potential-dependent outcomes from an EP Cu(100) electrode were detected during a cathodic LSV (black curves), followed by a normal pulse voltammetry (NPV, E_a=0.6V, t_a=t_c=1s and E_c swept from -0.5 to -1.2V, red curves). The HER is significantly suppressed whereas the ethanol/n-propanol formation is drastically enhanced under the NPV program in all the working potential range. Furthermore, the onset potential for HER is shifted to a more negative potential (-0.8V) during the NPV when compared to the LSV experiment (-0.6V), whereas the opposite occurs for the formation of ethanol/n-propanol (-0.6V vs -0.9V, respectively). The product selectivity measured at a lower reductive overpotential (E_c=-0.8V with E_a=0.6V, t_a=t_c=1s) is shown in Supplementary Figure 14, displaying a 2-fold increase of C_{2+} products under pulsed conditions (from 27.5 %to 57.5%, Supplementary Note 4).

Furthermore, the amount of ethylene and methane is more favored in the non-pulsed experiment, with only a slightly larger amount of ethylene detected at potentials more negative than -1.1V. However, the onset potential for the formation of both species is not affected. These results corroborate our previous findings that HER and C_1 product formation are more favored under non-pulsed conditions, whereas the formation of C_{2+}products is promoted by pulsing at E_a=0.6V.

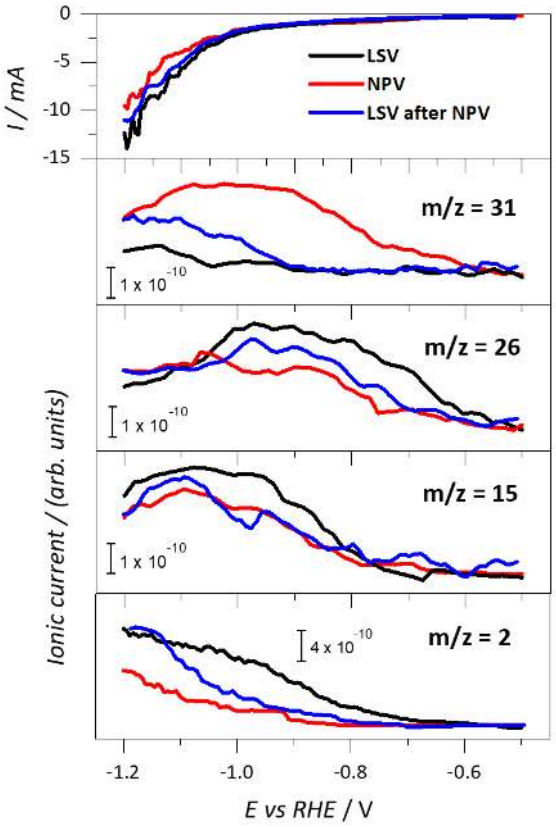

Figure 6. Differential electrochemical mass spectroscopy (DEMS) measurements. Simultaneously recorded LSV and volatile products for m/z = 2 (H_2), m/z = 15 (CH_3^+), m/z = 26 ($C_2H_2^+$) and m/z = 31(CH_3OH^+) in CO_2-saturated 0.1 M $KHCO_3$ solution at 5 mV s^{-1}.

It has been previously proposed that for the formation of C_1 products, CO has to adsorb first on Cu to form CHO_{ads} or COH_{ads} which should later react with adsorbed hydrogen (H_{ad})[49]:

$$COH_{ads}/CHO_{ads} + 5e^- + 5H^+ \rightarrow CH_4 + H_2O \qquad (1)$$

$$COH_{ads}/CHO_{ads} + 3e^- + 3H^+ \rightarrow CH_3OH \qquad (2)$$

However, when the amount of H_{ad} is suppressed due to the higher coverage of OH_{ads}, the amount of C-containing adsorbates increases, favoring their coupling to form $OCHCH_{2,ads}$, which can further reactto form ethylene:

$$OCHCH_{2,ads} + 3H^+ + 3e^- \rightarrow C_2H_4 + H_2O \qquad (3)$$

Nevertheless, $OCHCH_{2,ads}$ can also further hydrogenate to form $OCHCH_{3,ads}$ (4). This species can easily protonate to form ethanol or can react with other CO_{ads} to form n-propanol (5):

$$OCHCH_{3,ads} + 2H^+ + 2e^- \rightarrow C_2H_5OH \qquad (4)$$

$$OCHCH_{3,ads} + CO + 2H^+ + 6e^- \rightarrow n\text{-}C_3H_7OH + H_2O \quad (5)$$

Taking into account the lower intensity of the m/z=15 signal for NPV when compared with the LSV it is reasonable to assume that the pulses at E_a=0.6V favor the adsorption and dimerization of CO_{ads}. Furthermore, the prevalence of alcohol formation with respect to ethylene suggests that the intermediate $OCHCH_{2,ads}$ prefers to hydrogenate to form $OCHCH_{3,ads}$ rather than ethylene under pulsed conditions. These differences can be explained by the concomitant presence of Cu_2O when pulsing at E_a=0.6V. However, the presence of surface defects can also be at least partially responsible of the change in the distribution of the adsorbed species on the surface and thus, the different product selectivity.

To address this question, another LSV (Figure 6, blue line) was subsequently run after the NPV. As a result, the amount of hydrogen, methane and ethylene slightly increases when compared with the pulsed experiment. However, the amount of ethanol/n-propanol, despite being slightly higher than for the initial LSV, is much lower when compared with the NPV. Furthermore, the onset potential is very similar to that of the no-pulsed experiment on the less defective Cu(100) surface. Thus, the high similarity in the m/z=31 signal for the LSV before and after the NPV suggest that the high selectivity to ethanol/n-propanol during the pulsed experiment should be mostly attributed to the presence of Cu_2O, although as can be seen in Figure 4, the presence of defects also slightly influences the product distribution.

Conclusions

Our study provides in depth insight into the synergistic role of defects and specific structural motifs on Cu surfaces and Cu(I) species in the activity and selectivity of Cu(100) electrodes during CO_2 electroreduction. Significantly enhanced selectivity for ethanol has been found at -1.0V under pulsed electrolysis conditions where Cu(I) was continuously in situ (re)-generated by properly choosing the anodic potential applied. This finding has been further confirmed by the in situ detection of volatile products and intermediates during CO_2RR using DEMS. We propose that this catalytic enhancement is linked to the presence of specific structural motifs and surface Cu_2O which withstands the CO_2R pulse, as proved by quasi in situ XPS measurements.

Our findings suggest that the combination of (100) domains, defect sites, and surface Cu_2O is the best configuration to enhance the CO_2RR reaction pathway leading to C_{2+} products. In particular, the increased ethanol selectivity could be linked to the coexistence of Cu(I) and Cu^0 species, while the ethylene yield was dominated by the length of the Cu(100) terraces. The fundamental understanding shed by our study is remarkably valuable for rationally tailoring electrochemical interfaces with constrained surface structure and composition towards selective C_2 product production.

Methods

Electrode preparation. Cu(100) single crystal (MaTeck, 1 cm diameter, 99.999 %) was used as working electrode (WE). Before each experiment, the Cu single crystal was electropolished at 3 V vs Ti foil for 10 s in a H_3PO_4/H_2SO_4 solution consisting of 130 mL H_3PO_4 (VWR, 85 wt %), 20 mL H_2SO_4 (VWR, 95 %) and 60 mL ultrapure water (Elga, 18.2 MΩ cm). A commercial polycrystalline Cu foil (Advent Research Materials Ltd., 99.995 %) was used for comparison in the cyclic voltammetry experiments; in this case, it was electropolished for 3 min under the same conditions. Immediately after, all working electrodes were rinsed with ultrapure water and rapidly taken into the electrochemical cell.

Electrochemical characterization. Cu surfaces were electrochemically characterized at room temperature (RT) by cyclic voltammetry in Ar-saturated (Air Liquide, N50) 0.1 M NaOH (ACS. Reag. Merck) and 0.1 M $KHCO_3$ (99.9 %, Sigma-Aldrich) solutions at a sweep rate of 50 mV s^{-1} using the hanging meniscus configuration (Supplementary Figure 15a). The pH of these solutions are 8.8 and 13.1, respectively. An electrochemical cell with a three electrode configuration was employed, using a gold wire as a counter electrode and a reversible hydrogen electrode (RHE, HydroFlex, Gaskatel), attached to the cell through a Luggin capillary, as reference electrode. In this work, all potentials are referred to RHE. The electrode potential was controlled using a Biologic 240 potentiostat.

CO_2RR measurements. CO_2 electroreduction measurements were conducted with an Autolab potentiostat (Multi Autolab M204) in a custom-built glass H-cell, using an anion-exchange membrane

(Selemion AMV) to separate the anodic and the cathodic chambers, which were filled with 30 mL 0.1 M $KHCO_3$ solution each. A glass shield was built inside the cathodic semi-cell to prevent the breaking of the meniscus configuration used in the Cu single crystal measurements from the continuous CO_2 bubbling (Supplementary Figure 15b). A leak-free Ag/AgCl reference electrode (Innovative Instruments) and a Pt gauze counter electrode (MaTeck, 3600 mesh cm^{-2}) were used in a three electrode configuration. The 0.1 M $KHCO_3$ electrolyte was previously purified from trace metal ion impurities by using a cation-exchange resin (i.e., Chelex 100 resin, Bio-Rad) [50] , and subsequently saturated with CO_2 for 30 min. High purity CO_2 (Air Liquide, N45) was supplied using a calibrated mass flow controller (Bronkhorst) at a constant rate of 20 mL min^{-1} into the electrolyte, which was vigorously stirred during the electrochemical reaction. Prior to each measurement, a linear sweep voltammetry (LSV) was recorded, ensuring the total reduction of the EP electrode before the pulsed experiments. Potentiostatic measurements, i.e. with a constant voltage, were performed for reference at -1.0 V vs RHE on the Cu(100) electrode, showing that the FE for all identified major products is consistent with previous studies[14–16]. Throughout the paper, the selectivity data reported correspond to an average of at least three different measurements collected under the same experimental conditions, and the error bars represent the standard deviation.

Surface roughness. It was determined by measuring the double-layer capacitance of the electrode-electrolyte interface[49,50] for each electrode before (electropolished) and after pulse experiments at different scan rates (mV/s) in a CO_2-saturated 0.1M $KHCO_3$ solution. The capacitance can be calculated by the slope of the plot j vs υ using the equation:

$$C = \frac{Current\ density\ (j)}{Scan\ rate\ (\upsilon)}$$

The roughness factors were calculated using the equation:

$$Surface\ roughness = \frac{C}{C_0}$$

,where C is the capacitance of the Cu single crystal after each pulse experiment, and C_0 is the capacitance of the corresponding electropolished electrode.

Taking into consideration the small changes detected in the electrochemical surface roughness of the otherwise generally flat single crystal surfaces, we have used the geometric area to normalize the cyclic voltammograms and the measured current intensities.

Product analysis. The gaseous products formed during the reaction (i.e., hydrogen, CO, methane and ethylene) were quantified by gas chromatography (GC, Agilent 7890B) equipped with a thermal conductivity detector (TCD) and a flame ionization detector (FID). The GC was directly connected to the electrochemical cell for online analysis and gaseous samples were injected by a six-port valve. The first gas sample injection took place after 1 min of CO_2RR, followed by four additional GC measurements in 15 min intervals. Ethanol and n-propanol concentrations were analyzed by liquid GC (Shimadzu 2010 plus), equipped with a fused silica capillary column and a FID. Formate and acetate concentrations were quantified by high performance liquid chromatography (HPLC, Shimadzu Prominence) equipped with a NUCLEOGEL® SUGAR 810 column and refractive index detector (RID). All product selectivities reported in this paper were recorded after 1 h of CO_2RR.

Quasi in situ XPS. XPS measurements were performed before and directly after electrochemistry without exposing the sample to air. The electrochemical cell used is directly attached to the ultra-high vacuum (UHV) chamber, Supplementary Figure 16. For the XPS measurements, a commercial Phoibus100 (SPECS GmbH, E_{pass} = 15 eV) analyzer and XR 50 (SPECS GmbH) X-ray source (Al anode, P_{source} = 300 W) were used. All spectra were acquired in high resolution modus for at least 1 hour (depending on the region considered), using a step size of 0.05 eV, resulting in a total scan time of 75 min for Cu LMM Auger and 37 min for Cu 2p region. The Cu $2p_{3/2}$ peak was used to align the spectra to the binding energy of Cu/Cu_2O (E_{bin} = 932.67 eV) [51]. The Cu LMM Auger line was used to distinguish Cu from Cu^+ species. Cu_2O amount was estimated from the integrated area of the fit with the corresponding reference spectra. Reference spectra used to fit these data were acquired on a plasma oxidized-(CuO) sample and an in situ annealed & sputtered Cu foil (Cu^0). The reference Cu_2O spectrum

was taken from the literature[51]. The electrochemical measurements were carried out using an Autolab potentiostat (PGSTAT 302N) with a Pt mesh and a leak-free Ag/AgCl as counter and reference electrodes, respectively. All measurements were conducted at room temperature.

STM and AFM imaging. STM, XPS and UHV sample preparation were done in a UHV system with a base pressure better than $4x10^{-10}$ mbar. STM measurements were done with an STM 150 Aarhus HT microscope from SPECS GmbH. The electrochemical treatments of the samples were performed following the same procedure as described for the quasi in situ XPS measurements, Figure S13. AFM measurements in air were performed in tapping mode with a Bruker Multimode 8 microscope. After each experiment, the single crystal surface was recovered following a three-step process. First, short electropolishing (20 s) to perform a coarse cleaning. After copiously rinsing with ultrapure water and drying with inert gas, the samples were then transferred to the UHV system. The final treatment consisted of cycles of sputtering with Ar^+-ions ($p_{Ar} = 3x10^{-5}$ mbar, $E_{kin} = 2.5$ keV, 15-30 min) and subsequent annealing at 650-700 °C in UHV for 10-15 min until a flat surface with satisfying morphology could be seen in STM.

DEMS measurements. DEMS studies were carried out to *in situ* detect the formation of volatile products and intermediates as a function of the applied potential, and compare this "on-line" product distribution with the "accumulative" product analysis after 1 h of CO_2RR electrolysis. These experiments were conducted by using a Hiden HPR-40 quadrupole mass spectrometer (Hiden Analytical) coupled to a single thin layer flow cell (Hiden Analytical). A leak-free Ag/AgCl, a Pt wire and a 7mm diameter Cu(100) single-crystal were used as reference, counter and working electrodes, respectively. A Teflon membrane (Cat. No. PF-003HS for Cobetter® porous size 30 nm) was employed in order to detect only volatile, especially if hydrophobic products and intermediates were formed during the reaction. The Teflon membrane was located in between the electrochemical cell and the mass spectrometer port and positioned close to the working electrode (few millimeters). An electron energy of 70 eV was employed for ionization of the different detected species using an emission current of 500 μA. The hydrogen ions produced were accelerated with a voltage of 1.3 V and the other ions were

accelerated with a voltage of 3 V in order to avoid detector saturation with hydrogen ions and optimize the detector response for the other species. The secondary electron multiplier (SEM) energy was set to 1200 V for all species detected.

Data availability

The main data supporting the findings of this study are available within the article and its Supplementary Information. Additional data are available from the corresponding authors on reasonable request.

Acknowledgements

This work was supported by the European Research Council under grant ERC-OPERANDOCAT (ERC-725915) and the German Federal Ministry of Education and Research (BMBF) under grants #033RCOO4D-'e-Ethylene' and #03SF0523C-'CO2EKAT'. S.K. acknowledges financial support from the Max Planck Research School for Interface Controlled Materials for Energy Conversion (IMPRS-SurMat). Funding from the Deutsche Forschungsgemeinschaft (DFG, German Research Foundation) under Germany´s Excellence Strategy – EXC 2008/1 (UniSysCat) – 390540038 is also appreciated.

Author contributions

R.M.A.A. designed the electrochemical experiments, analyzed the results and wrote the manuscript. F.S. performed the quasi *in situ* XPS measurements and wrote the corresponding section. S.K. carried out the microscopic characterization by STM and AFM. R.R. performed the DEMS experiments and wrote the corresponding section. B.R.C. co-designed the experiments, guided and supervised the project and co-wrote the manuscript. All authors discussed the results and reviewed the manuscript.

Competing interests

The authors declare no competing interest.

Additional information

Supplementary information is available.

References

1. Seh, Z. W. *et al.* Combining theory and experiment in electrocatalysis: Insights into materials design. *Science (80-.).* **355**, eaad4998 (2017).
2. Zhang, W. *et al.* Progress and Perspective of Electrocatalytic CO2 Reduction for Renewable Carbonaceous Fuels and Chemicals. *Adv. Sci.* **5**, 1700275 (2018).
3. Hori, Y. Electrochemical CO2 Reduction on Metal Electrodes. *Mod. Asp. Electrochem.* **42**, 89–189 (2008).
4. Gattrell, M., Gupta, N. & Co, A. A review of the aqueous electrochemical reduction of CO2 to hydrocarbons at copper. *J. Electroanal. Chem.* **594**, 1–19 (2006).
5. Gao, D., Arán-Ais, R. M., Jeon, H. S. & Roldan Cuenya, B. Rational catalyst and electrolyte design for CO2 electroreduction towards multicarbon products. *Nat. Catal.* **2**, 198–210 (2019).
6. Singh, M. R., Clark, E. L. & Bell, A. T. Thermodynamic and achievable efficiencies for solar-driven electrochemical reduction of carbon dioxide to transportation fuels. *Proc. Natl. Acad. Sci.* **112**, E6111–E6118 (2015).
7. Schouten, K. J. P., Kwon, Y., van der Ham, C. J. M., Qin, Z. & Koper, M. T. M. A new mechanism for the selectivity to C1 and C2 species in the electrochemical reduction of carbon dioxide on copper electrodes. *Chem. Sci.* **2**, 1902–1909 (2011).
8. Peterson, A. A., Abild-Pedersen, F., Studt, F., Rossmeisl, J. & Nørskov, J. K. How copper catalyzes the electroreduction of CO2 into hydrocarbon fuels. *Energy Environ. Sci.* **3**, 1311–1315 (2010).
9. Arán-Ais, R. M., Gao, D. & Roldan Cuenya, B. Structure- and Electrolyte-Sensitivity in CO2 Electroreduction. *Acc. Chem. Res.* **51**, 2906–2917 (2018).
10. Durand, W. J., Peterson, A. A., Studt, F., Abild-Pedersen, F. & Nørskov, J. K. Structure effects on the energetics of the electrochemical reduction of CO2 by copper surfaces. *Surf. Sci.* **605**, 1354–1359 (2011).
11. Montoya, J. H., Shi, C., Chan, K. & Nørskov, J. K. Theoretical Insights into a CO Dimerization

Mechanism in CO_2 Electroreduction. *J. Phys. Chem. Lett.* **6**, 2032–2037 (2015).

12. Calle-Vallejo, F. & Koper, M. T. M. Theoretical considerations on the electroreduction of CO to C2 Species on Cu(100) electrodes. *Angew. Chemie Int. Ed.* **52**, 7282–7285 (2013).
13. Bagger, A., Ju, W., Varela, A. S., Strasser, P. & Rossmeisl, J. Electrochemical CO2 Reduction: Classifying Cu Facets. *ACS Catal.* **9**, 7894–7899 (2019).
14. Hori, Y., Takahashi, I., Koga, O. & Hoshi, N. Selective Formation of C2 Compounds from Electrochemical Reduction of CO2 at a Series of Copper Single Crystal Electrodes. *J. Phys. Chem. B* **106**, 15–17 (2002).
15. Hori, Y., Takahashi, I., Koga, O. & Hoshi, N. Electrochemical reduction of carbon dioxide at various series of copper single crystal electrodes. *J. Mol. Catal. A Chem.* **199**, 39–47 (2003).
16. Huang, Y., Handoko, A. D., Hirunsit, P. & Yeo, B. S. Electrochemical Reduction of CO2 Using Copper Single-Crystal Surfaces: Effects of CO* Coverage on the Selective Formation of Ethylene. *ACS Catal.* **7**, 1749–1756 (2017).
17. Zhou, Y. *et al.* Dopant-induced electron localization drives CO2 reduction to C2 hydrocarbons. *Nat. Chem.* **10**, 974–980 (2018).
18. Eilert, A. *et al.* Subsurface Oxygen in Oxide-Derived Copper Electrocatalysts for Carbon Dioxide Reduction. *J. Phys. Chem. Lett.* **8**, 285–290 (2017).
19. Xiao, H., Goddard, W., Cheng, T. & Liu, Y. Cu metal embedded in oxidized matrix catalyst to promote CO2 activation and CO dimerization for electrochemical reduction of CO2. *Proc. Natl. Acad. Sci.* **114**, 6685–6688 (2017).
20. Mistry, H. *et al.* Highly selective plasma-activated copper catalysts for CO2 reduction to ethylene. *Nat. Commun.* **7**, 12123 (2016).
21. Gao, D. *et al.* Plasma-Activated Copper Nanocube Catalysts for Efficient CO2 Electroreduction to Hydrocarbons and Alcohols. *ACS Nano* **11**, 4825–4831 (2017).
22. Handoko, A. D. *et al.* Mechanistic insights into the selective electroreduction of carbon dioxide to ethylene on Cu2O-derived copper catalysts. *J. Phys. Chem. C* **120**, 20058–20067 (2016).
23. Ren, D. *et al.* Selective Electrochemical Reduction of CO2 to Ethylene and Ethanol on Copper(I) oxide catalysts. *ACS Catal.* **5**, 2814–2821 (2015).

24. De Luna, P. *et al.* Catalyst electro-redeposition controls morphology and oxidation state for selective carbon dioxide reduction. *Nat. Catal.* **1**, 103–110 (2018).

25. Le Duff, C. S., Lawrence, M. J. & Rodriguez, P. Role of the adsorbed oxygen species in the selective electrochemical reduction of CO2 to alcohols and carbonyls on copper electrodes. *Angew. Chemie Int. Ed.* **56**, 12919–12924 (2017).

26. Gao, D., Scholten, F. & Roldan Cuenya, B. Improved CO2 Electroreduction Performance on Plasma-Activated Cu Catalysts via Electrolyte Design: Halide Effect. *ACS Catal.* **7**, 5112–5120 (2017).

27. Kimura, K. W. *et al.* Controlled Selectivity of CO2 Reduction on Copper by Pulsing the Electrochemical Potential. *ChemSusChem* **11**, 1781–1786 (2018).

28. Lim, C. F. C., Harrington, D. A. & Marshall, A. T. Altering the selectivity of galvanostatic CO2 reduction on Cu cathodes by periodic cyclic voltammetry and potentiostatic steps. *Electrochim. Acta* **222**, 133–140 (2016).

29. Kumar, B. *et al.* Controlling the Product Syngas H2:CO Ratio through Pulsed-Bias Electrochemical Reduction of CO2 on Copper. *ACS Catal.* **6**, 4739–4745 (2016).

30. Yano, J. & Yamasaki, S. Pulse-mode electrochemical reduction of carbon dioxide using copper and copper oxide electrodes for selective ethylene formation. *J. Appl. Electrochem.* **38**, 1721 (2008).

31. Jermann, B. & Augustynski, J. Long-term activation of the copper cathode in the course of CO2 reduction. *Electrochim. Acta* **39**, 1891–1896 (1994).

32. Shiratsuchi, R., Aikoh, Y. & Nogami, G. Pulsed Electroreduction of CO2 on Copper Electrodes. *J. Electrochem. Soc.* **140**, 3479–3482 (1993).

33. Engelbrecht, A. *et al.* On the Electrochemical CO2 Reduction at Copper Sheet Electrodes with Enhanced Long-Term Stability by Pulsed Electrolysis. *J. Electrochem. Soc.* **165**, J3059–J3068 (2018).

34. Velasco-Vélez, J.-J. *et al.* The Role of the Copper Oxidation State in the Electrocatalytic Reduction of CO2 into Valuable Hydrocarbons. *ACS Sustain. Chem. Eng.* **7**, 1485–1492 (2019).

35. Engstfeld, A. K., Maagaard, T., Horch, S., Chorkendorff, I. & Stephens, I. E. L. Polycrystalline and Single-Crystal Cu Electrodes: Influence of Experimental Conditions on the Electrochemical Properties in Alkaline Media. *Chem. – A Eur. J.* **24**, 17743–17755 (2018).

36. Kim, Y.-G. *et al.* Surface reconstruction of pure-Cu single-crystal electrodes under CO-reduction potentials in alkaline solutions: A study by seriatim ECSTM-DEMS. *J. Electroanal. Chem.* **780**, 290–295 (2016).

37. Kim, Y.-G., Baricuatro, J. H. & Soriaga, M. P. Surface Reconstruction of Polycrystalline Cu Electrodes in Aqueous KHCO3 Electrolyte at Potentials in the Early Stages of CO2 Reduction. *Electrocatalysis* **9**, 526–530 (2018).

38. Kim, Y.-G., Baricuatro, J. H., Javier, A., Gregoire, J. M. & Soriaga, M. P. The Evolution of the Polycrystalline Copper Surface, First to Cu(111) and Then to Cu(100), at a Fixed CO2RR Potential: A Study by Operando EC-STM. *Langmuir* **30**, 15053–15056 (2014).

39. Protopopoff, E. & Marcus, P. Potential–pH diagrams for hydroxyl and hydrogen adsorbed on a copper surface. *Electrochim. Acta* **51**, 408–417 (2005).

40. P. Schouten, K. J., Gallent, E. P. & Koper, M. T. M. The electrochemical characterization of copper single-crystal electrodes in alkaline media. *J. Electroanal. Chem.* **699**, 6–9 (2013).

41. Schouten, K. J. P., Pérez Gallent, E., Koper, M. T. M. & Schouten, K., Gallent, E., Koper, M. Structure Sensitivity of the Electrochemical Reduction of Carbon Monoxide on Copper Single Crystals. *ACS Catal.* **3**, 1292–1295 (2013).

42. Mariano, R. G., McKelvey, K., White, H. S. & Kanan, M. W. Selective increase in CO2 electroreduction activity at grain-boundary surface terminations. *Science (80-.).* **358**, 1187–1192 (2017).

43. Kas, R. *et al.* Electrochemical CO2 reduction on Cu2O-derived copper nanoparticles: controlling the catalytic selectivity of hydrocarbons. *Phys. Chem. Chem. Phys.* **16**, 12194–12201 (2014).

44. Tang, W. *et al.* The importance of surface morphology in controlling the selectivity of polycrystalline copper for CO2 electroreduction. *Phys. Chem. Chem. Phys.* **14**, 76–81 (2012).

45. Trasatti, S. & Petrii O, A. Real surface area measurements in electrochemistry. *Pure and*

Applied Chemistry **63**, 711 (1991).

46. Clark, E. L. *et al.* Standards and Protocols for Data Acquisition and Reporting for Studies of the Electrochemical Reduction of Carbon Dioxide. *ACS Catal.* **8**, 6560–6570 (2018).

47. Hagman, B. *et al.* Steps Control the Dissociation of CO2 on Cu(100). *J. Am. Chem. Soc.* **140**, 12974–12979 (2018).

48. Hahn, C. *et al.* Engineering Cu surfaces for the electrocatalytic conversion of CO2 : Controlling selectivity toward oxygenates and hydrocarbons. *Proc. Natl. Acad. Sci.* **114**, 5918–5923 (2017).

49. Kortlever, R., Shen, J., Schouten, K. J. P., Calle-Vallejo, F. & Koper, M. T. M. Catalysts and Reaction Pathways for the Electrochemical Reduction of Carbon Dioxide. *J. Phys. Chem. Lett.* **6**, 4073–4082 (2015).

50. Wuttig, A. & Surendranath, Y. Impurity Ion Complexation Enhances Carbon Dioxide Reduction Catalysis. *ACS Catal.* **5**, 4479–4484 (2015).

51. Biesinger, M. C. Advanced analysis of copper X-ray photoelectron spectra. *Surf. Interface Anal.* **49**, 1325–1334 (2017).